A liquid hydrogen target for radioactive beam experiments using the missing mass method

S. Koyama, D. Suzuki, M. Assié, N. Kitamura, L. Lalanne, M. Niikura, H. Otsu, T.Y. Saito, O. Sorlin

Version of Record: https://www.sciencedirect.com/science/article/pii/S0168900221004629
Manuscript_04a27eea25de871babe4401a192d5e33

A liquid hydrogen target for radioactive beam experiments using the missing mass method

S. Koyama[1,2,*], D. Suzuki[3], M. Assié[4], N. Kitamura[5], L. Lalanne[4], M. Niikura[1], H. Otsu[3], T. Y. Saito[1], O. Sorlin[2]

[1] *Department of Physics, the University of Tokyo, Hongo 7-3-1, Bunkyo, Tokyo 113-0033, Japan*
[2] *Grand Accélérateur National d'Ions Lourd (GANIL),CEA/DRF-CNRS/IN2P3, Bd. Henri Becquerel, 14076 Caen, France*
[3] *RIKEN Nishina Center, Hirosawa 2-1, Wako, Saitama 351-0198, Japan*
[4] *Université Paris-Saclay, CNRS/IN2P3, IJCLab, 91405 Orsay, France*
[5] *Center for Nuclear Study, the University of Tokyo, Hongo 7-3-1, Bunkyo, Tokyo 113-0033, Japan*

Abstract

We developed a liquid hydrogen target dedicated to missing mass spectroscopy using radioactive isotope beams. The target has a circular aperture of 20 mm and a maximum thickness of 1.5 mm at the center. A test experiment with a ^{12}C beam at 54.4 MeV/u was performed at GANIL. The ^{12}C$(p,d)^{11}$C reaction was measured with the charged-particle telescopes MUST2. An excitation energy resolution of 500-keV r.m.s. was obtained for the observed ground state. The target thickness was confirmed from the comparison of the measured differential cross sections to previous measurements.

Keywords: Liquid hydrogen target, Radioactive ion beam, Missing mass spectroscopy

1. Introduction

Radioactive isotopes often manifest unique phenomena that would be unexpected with stable nuclei, such as the halo structure [1] or the disappearance of magic numbers [2]. Radioactive isotope (RI) beam facilities, which provide radioactive isotopes in the form of beams, have been a driving force to investigate the structure and reactions of unstable nuclei. New generations of RI beam facilities are presently under construction [3–7] or in operation [8] across the world.

In this paper, we report on our development of a liquid hydrogen target for proton induced reactions of RI beams. In scattering experiments, protons are often used as a probe. Proton induced reactions have relatively simple reaction mechanisms and better known optical potentials than other heavier targets. The reaction formalisms such as the DWBA or DWIA are known to be applicable and various reaction codes (DWUCK4/5 [9], TWOFNR [10], FRESCO [11]) have been developed to calculate cross sections and other reaction observables. Inelastic proton scattering or the one-neutron transfer (p,d) reaction are thus established reaction probes sensitive to the collectivity or single particle nature of nuclei of interest. The combined use of a liquid hydrogen target and RI beams allows to investigate the inherent structure of radioactive isotopes.

Various cryogenic hydrogen targets [12–20] have been developed for spectroscopy of RI beams. We summarize existing cryogenic targets in Fig. 1 as a function of opening areas and areal densities. Most of the early types of cryogenic hydrogen targets are found at the thicker and wider end of the distribution ($> 10^2$ mg/cm^2 and 1 cm^2). These targets are optimized to increase the luminosity or experimental yields by compensating lower beam intensities (typically less than 10^5 particles per second) with a number of hydrogen atoms and efficiently accepting an RI beam with a large profile (1-10 cm^2). While spectroscopy is often carried out with the detection of gamma-rays, neutrons, or fast ions that are transmissive, these thick targets are not optimal for spectroscopy utilizing low energy ions with high stopping powers in a medium.

Our liquid hydrogen target has been developed to perform the so-called missing mass spectroscopy with RI beams, as indicated by the red star in Fig. 1. Note that our reactions of interest are mostly direct reactions at 10 to 100 MeV/u and do not include quasi free scattering at higher energies. In the missing mass method,

*Corresponding author
Email address: shumpei.koyama@ganil.fr (S. Koyama)

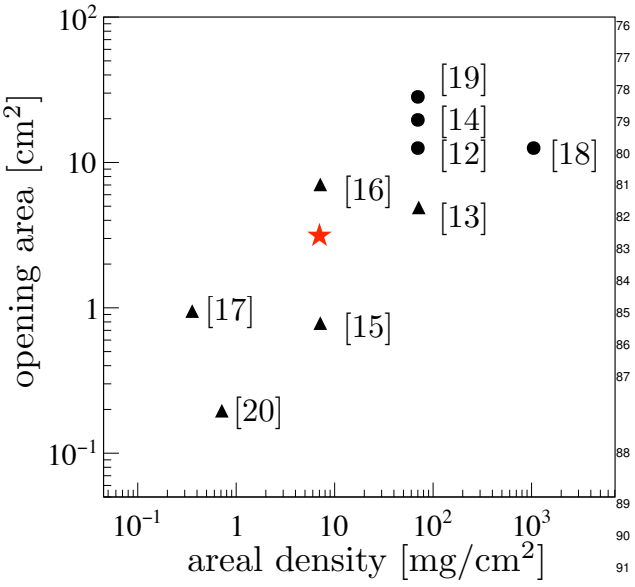

Figure 1: The opening area and areal density of cryogenic hydrogen targets. The available thinnest areal density of each target system is shown. The liquid and solid hydrogen targets are indicated by the circles and triangles with reference numbers, respectively. The liquid hydrogen target of this work is highlighted by the red star.

the excitation energies and angular distributions are obtained from the energy and emission angle of the recoiling ions. An advantage of this method is that the information of the nucleus of interest can be obtained only from the recoiling ion without detecting the nucleus or any of its decay products. While missing mass experiments with RI beams [21–25] have been carried out with silicon detector arrays optimized for the detection of low energy ions such as MUST [26], MUST2 [27], HiRA [28], HELIOS [29] or TiARA [30], most of these experiments are limited to RI beams with relatively high intensity. The difficulty in adopting this method to RI beams is that the recoiling ions are often emitted at low energies in the laboratory frame, typically 10 MeV or less in the region of interest. The high stopping power imposes a constraint on the target thickness. Several previous targets developed for missing mass experiments are thus found at the thinner end of Fig. 1. However, the size of the entrance window of these targets is usually small to limit the heat capacity of the target and its tendency to warm up under thermal radiation. This is because a thinner target has a smaller heat capacity with a large entrance window and is more prone to warm up under thermal radiation. To limit the warming due to thermal radiation, the opening area is limited to 1 cm^2 or smaller. This inevitably leads to a loss of acceptance when RI beams have a large beam profile.

The goal of the present development is to realize a cryogenic hydrogen target of a thin thickness (about 1 mm), and with a reasonably large aperture (3.14 cm^2) for missing mass experiments with RI beams. The target was realized in the liquid phase, not in the solid for easier handling of the target and vacuum system.
The requirements of hydrogen targets for the missing mass experiments are described in Section 2. The description of the target system including the newly designed target cells is summarized in Section 3. In Section 4, the test experiments with the new target cell is presented. Finally, conclusion is given in Section 5.

2. Requirements of hydrogen targets

In this section, we describe the specifications of our liquid hydrogen target. CH_2 foils are the most readily available solution for proton targets. While CH_2 has good mechanical and thermodynamical characteristics at room temperature, the typical areal density of hydrogen for the application of missing mass spectroscopy is as low as 1 mg/cm^2, or 12.5 μm thickness. This is because CH_2 contains carbon atoms which reduce the number of hydrogen atoms per unit length. Under the condition that the energy loss of an ion traversing the medium is equivalent, the number of hydrogen atoms in solid or liquid hydrogen targets is about 5 times larger than in CH_2 targets. This is the advantage of using a cryogenic target albeit its realization and operation are much more difficult than for a CH_2 target.
In terms of density, liquid and solid hydrogen are almost the same. The density of liquid hydrogen, 7.0 mg/cm^3 at 18 K and 1 atm, is as large as that of solid hydrogen, 7.15 mg/cm^3. To efficiently accept RI beam ions from the projectile fragmentation reaction with a spot size of 1 to 10 cm^2, a larger aperture size is desirable. The downside in enlarging the aperture is that the heat radiation through the larger surface area makes it harder to maintain the liquid or solid phase. From this point of view, a liquid hydrogen target has a practical advantage over a solid hydrogen target, since the critical temperature of the liquid phase (21 K) is higher than that of the solid phase (14 K).
For a better excitation energy resolution with reactions with low energy recoiling particles, the angular and energy straggling in the target should be small. This is because the straggling deteriorates the resolution of the kinetic energy and the scattering angle of a recoiling particle. In addition, the energy loss inside the target adds to the uncertainty of measured energies, which is increasingly important as the energy decreases. Later in Sect. 4, we will show the test result of the ^{12}C$(p, d)^{11}$C

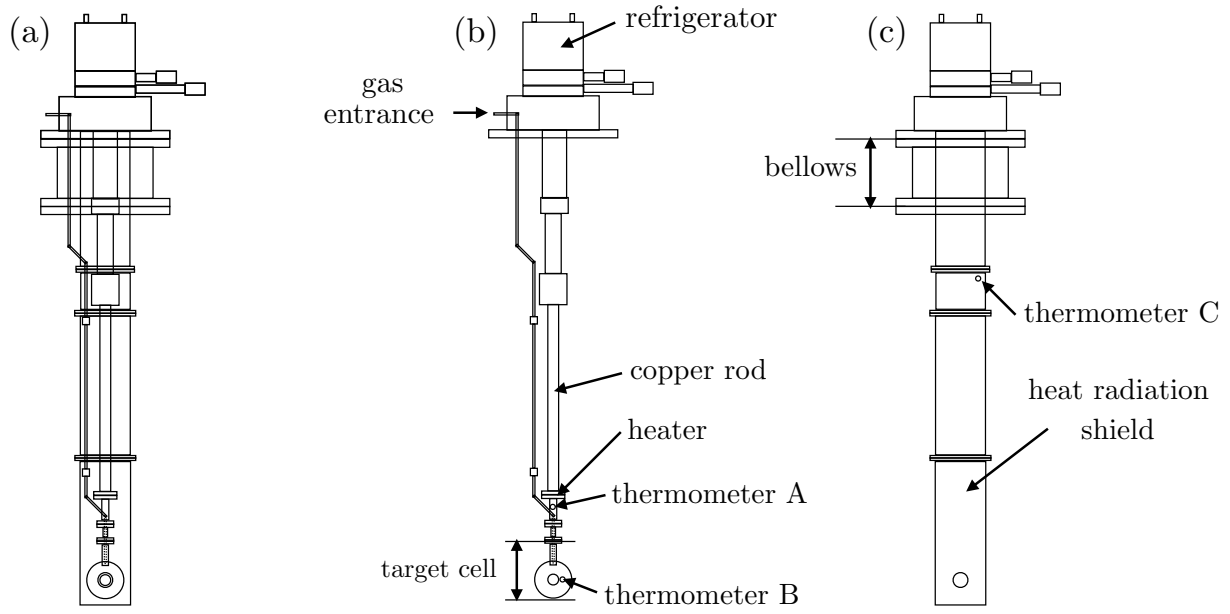

Figure 2: (a) Schematic drawing of the CRYPTA system. (b) Only the parts connected to the first cooling stage of the refrigerator are displayed. (c) The other parts connected to the second cooling stage.

reaction at 54.4 MeV/u as a typical reaction of our interest. Deuterons are emitted at forward angles with an energy of 18 MeV or higher (Fig. 11). With a liquid hydrogen target of 1 mm thickness, the energy loss of an 18 MeV deuteron while traversing half the target is estimated to be 413 keV. This uncertainty balances with the energy resolution of CsI(Tl) detector (a few hundred keV r.m.s.), which is often used to measure the kinetic energy of a recoiling particle.

With these considerations, we developed a thin liquid hydrogen target of about 1-mm thickness while keeping the aperture size as large as possible. We realized an aperture of 20 mm in diameter and a measured thickness of 1.5 mm at the center with deformed window foils.

3. Description of the system

In this development, we used the cryogenic target system CRYPTA [14]. CRYPTA is a target system that has routinely been operated at the Radioactive Isotope Beam Factory (RIBF) of RIKEN to provide proton and deuteron targets to various experiments of in-beam γ-ray spectroscopy or invariant mass spectroscopy using RI beams [31–35]. The advantage of CRYPTA is that the target cell has a modular construction and is detachable from the cooling rod. The shape and dimensions can be optimized depending on the requirements. In the previous experiments, target cells with a thickness of 10 mm or larger were adopted. We developed a cell optimized for the present purpose.

3.1. Overview of the cryogenic target system

A schematic view of CRYPTA is shown in Fig. 2. A Gifford-McMahon cycle refrigerator is used for cooling. A target cell is connected to the refrigerator with a copper rod in a vacuum chamber. The target cell and the copper rod are surrounded by an aluminum shield, called heat radiation shield hereafter, to protect the cold parts from thermal radiation emitted by the materials at room temperature, most importantly the wall of the vacuum chamber. The target cell, copper rod and heat radiation shield are kept under vacuum. The refrigerator is attached to the top of the vacuum chamber. The system and the top flange of the vacuum chamber are connected by a bellows. The position of the target cell can be optimized by adjusting this bellows. The refrigerator has two cooling contacts with different capacities. The first stage, to which the heat radiation shield is attached, reaches the lowest temperature of 38 K with a capacity of 9 W. The second stage is connected to the target cell via the copper rod. This stage with a capacity of 5 W reaches the lowest temperature of 10 K. For the adiabatic cooling, helium gas with a purity of 99.999% at a pressure of 10 atm is used. The compression and heat exchange of the gas are performed by the compressor CW303 of Iwatani Cooperation. The gas

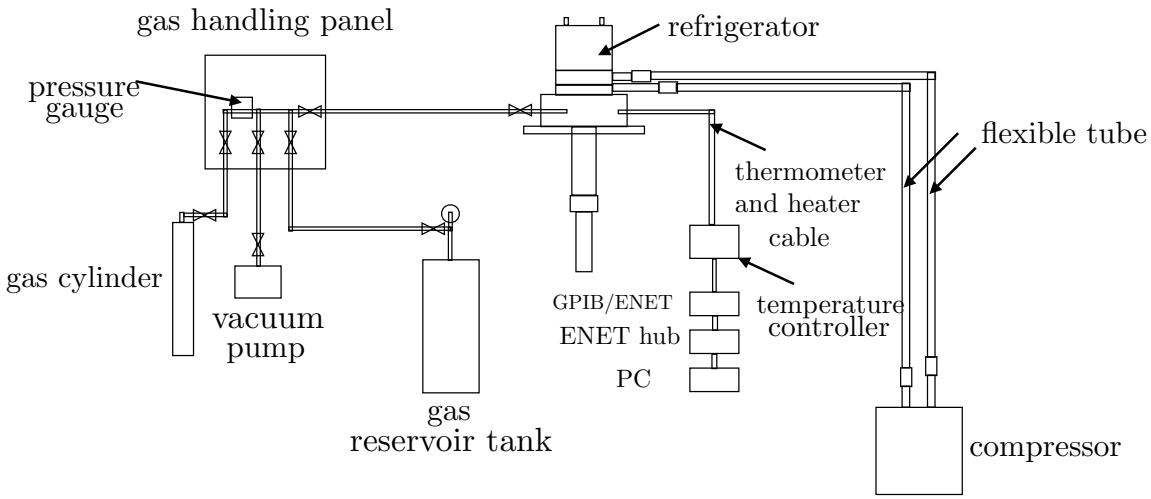

Figure 3: Schematic drawing of the vacuum and gas equipment and the monitoring devices.

circulates in a closed system consisting of the refrigerator and the compressor connected via a pair of stainless steel flexible tubings. The compressor was cooled by tap or chilled water at temperatures between 10°C to 25°C.

A schematic drawing of the vacuum and gas tubings is shown in Fig. 3. The operation and control of the vacuum and hydrogen gas were manually carried out by using a dedicated gas handling panel. All volumes (target cell, reservoir tank, hydrogen gas cylinder), pumping and monitoring devices are connected to or integrated into this panel. The reservoir tank serves as a buffer to store hydrogen gas when the target cell is empty. By opening the outlet valve, hydrogen gas is channeled to the target cell. When needed, additional gas can be supplied from the gas cylinder to the reservoir. To monitor the temperatures, three DT-470 silicon diode cryogenic temperature sensors of Lake Shore Cryotronics, Inc. are used. One of the thermometers is attached to the upper part of the target cell hereafter called 'thermometer A', another to the location near the aperture on the front surface of the target cell (thermometer B) and the last one to the heat radiation shield (thermometer C). Thermometer A and C are permanently fixed with solder. Thermometer B is attached by a high-vacuum grease APIEZON N to facilitate the detachment when the target cell windows are changed. A 30 Ω thermocouple is used as a heater. The heater is attached to the copper rod close to thermometer A. The heater is used to prevent liquid hydrogen from being solidified during cooling and to evaporate liquid hydrogen during warming. The thermometers and the heater are connected to the cryogenic temperature controller model 331 of Lake Shore Cryotronics, Inc. The heater power was continuously adjusted by the so-called PID control [36]. The PID control is a feedback control method to keep a given value, the temperature of thermometer A in the current case, constant. For this purpose, the proportional (P), integral (I) and derivative (D) of the difference of the current value and the set value ($e(t)$) as a function of time (t) are used. The manipulated variable, the heater power in the current case, is given by $K_P e(t) + K_I \int_0^t e(t')\mathrm{d}t' + K_D \mathrm{d}e(t)/\mathrm{d}t$. The coefficients were set $K_P = 10$, $K_I = 70$ /s and $K_D = 10$ s. The module was remotely monitored and controlled via GPIB control. The GPIB output was connected to the Ethernet network by the GPIB/ENET/100 module of National Instruments. A LabVIEW based software was used to set and write the parameters of the module, or monitor and record the outputs of the thermometers. The recording interval was set to be five seconds. The module was also controlled by a computer placed outside of the experimental area.

3.2. Target cell

The target cell consists of a body frame and a pair of windows, all made of the A6061 aluminum alloy, which has a high thermal conductivity of 0.15 kW/(m°C) at

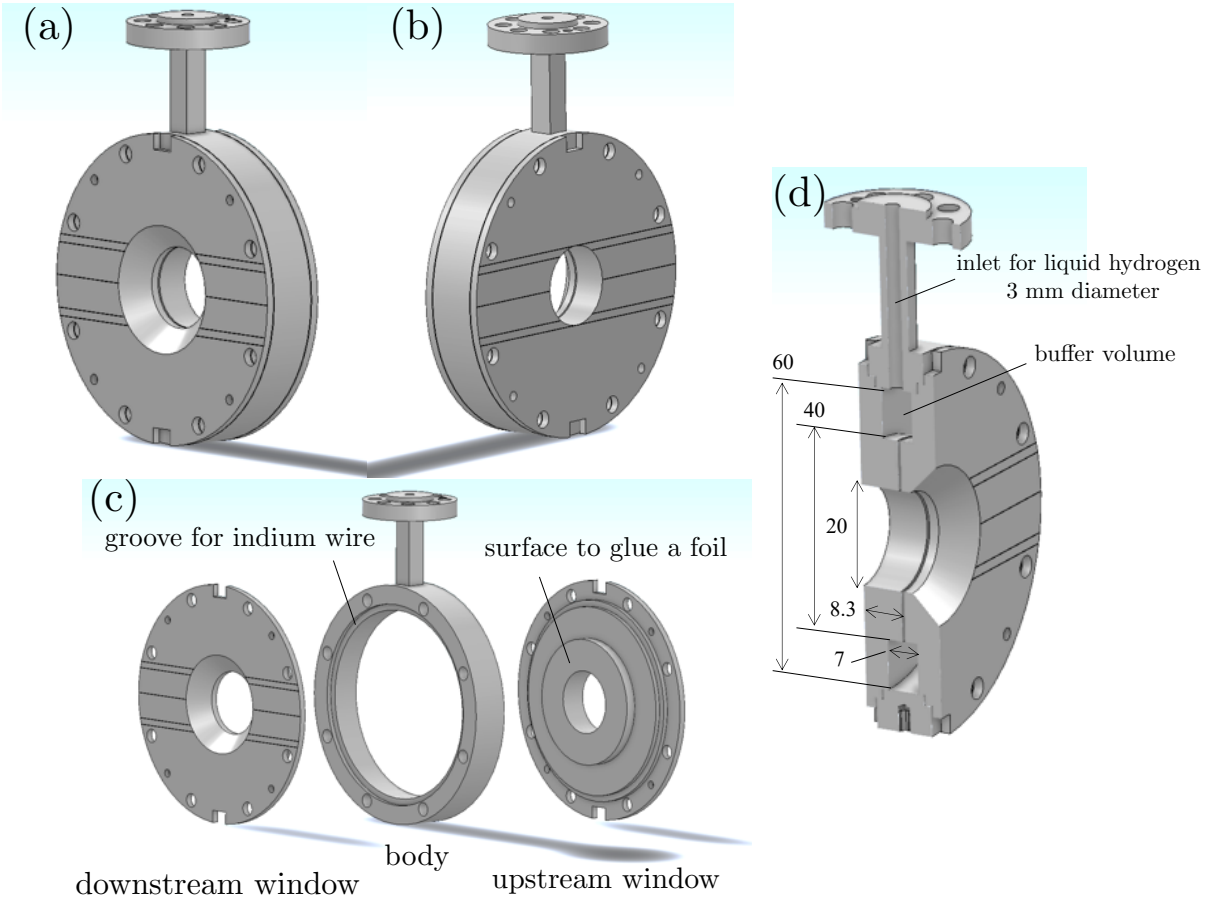

Figure 4: Schematic drawings of the assembled target cell seen from (a) downstream and (b) upstream. (c) An expanded view of the body and windows. (d) A cross sectional side view of the target cell. All dimensions are given in mm.

25°C. Schematic drawings of the target cell are shown in Fig. 4. A 3-mm diameter inlet of the hydrogen gas was made inside the attachment to the copper rod. Each window had an aperture of 20 mm in diameter at the center where beam particles were transmitted. The aperture of the downstream window was tapered at 45° so that the outer edge of the aperture would not intercept particles scattered at large angles, thus increasing the angular coverage. The upstream window was not tapered. Beam particles were intercepted by the flat surface around the aperture with aluminum of 8.3 mm in thickness. This minimizes the risk of these particles directly hitting the detectors around the target. A 6.47-μm-thick HAVAR foil was glued to each window with Stycast 1266 epoxy resin of Henkel Loctite, which keeps good adhesion under high vacuum at low temperatures. An advantage of HAVAR foils over organic compound alternatives is its stiffness. The elastic modulus of HAVAR is 200 GPa [37] while that of Kapton, a widely used organic compound foil, is 3 GPa at room temperature. The foils were attached to the inner surfaces of the windows to withstand the outward pressure from liquid and gaseous hydrogen inside. The target cell was assembled with eight screws. To ensure tight sealing against liquid hydrogen, a 1-mm-diameter indium wire was inserted between the contacting surfaces of the body frame and a window. By tightening the screws, the indium wires on both sides are compressed to establish intimate contact. The designed distance between the foils of the two windows was 0.5 mm. As seen in the cross sectional view in Fig. 4, the target cell thus assembled has a buffer volume of liquid hydrogen with a thickness of 7 mm surrounding the opening area. During filling, liquid hydrogen from the inlet at the top first fills the buffer volume. Once the buffered liquid has enough pressure, it starts leaking into the aperture volume through the peripheral slit as narrow as 0.5 mm.

3.3. Measurement of the uniformity of the window foils

The uniformity of the target surface is an important property of the cryogenic target for reaction studies since inhomogeneous target thickness often consti-

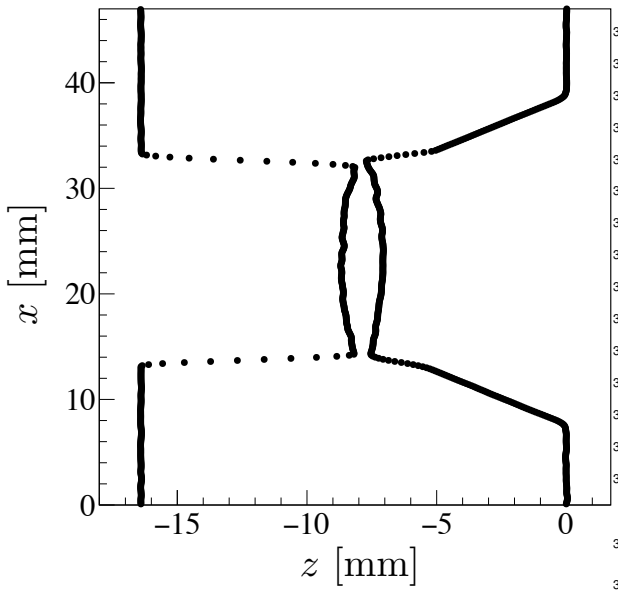

Figure 5: Surfaces of the target window foils scanned by a laser sensor. The cell was filled with hydrogen gas at 0.8 atm and put under vacuum.

tutes a major source of uncertainties in deducing reaction cross sections. To limit the inhomogeneity, many efforts have been made for the existing hydrogen targets as summarized in Ref. [38]. For liquid hydrogen targets, one way is to use a foil with high elastic modulus to mitigate the bulge under the outward pressure of liquid albeit it adds impurities to the target (see also Fig. 28 of Ref. [38]). In the present case, a foil of HAVAR with high elastic modulus was used. While the thickness of 6.47 μm ensures that the number of impurities (5.56×10^{19}/ cm^2) is much lower with respect to the hydrogen target of 1 mm in thickness (4.18×10^{21} /cm^2), it efficiently limits the flat surface to bulge. To evaluate the uniformity of the target surfaces, we measured the size of displacement at each point of the surface by using the laser displacement sensor LK-500 of Keyence. The device is a laser-based technology to measure the distance from an object with an accuracy of 0.1 mm. In the measurement, the target cell was put in a vacuum chamber with a diameter of 15 cm. The chamber has a glass view port at 11.5 cm from the target cell window. A beam of laser light from the LK-500 device was directed toward the target cell through this view port. We scanned the surface of each window foil by stepping the LK-500 device in the vertical direction. For simplicity, the target cell was filled with hydrogen gas at 0.8 atm and at room temperature. The results of the front and back surfaces are shown together in Fig. 5. The pair of foils is separated by the designed distance of 0.5 mm at the periphery of the aperture. It was found that the foils gradually swelled outwards from the edge to the center. The maximum size of displacement was 0.5 mm at the center of the aperture. The total thickness of liquid hydrogen is 1.5 mm, larger by 1 mm with respect to the periphery of the aperture, where the size of 0.5 mm is defined by the distance of the opposing target windows. The volume inside the opening is estimated to 100π mm^3 by approximating the shapes of the foils with a quadratic function. This volume translates into an average thickness of 1.0 mm given the opening area of 100π mm^2 assuming a uniform beam profile. The corresponding areal density of liquid hydrogen is 7.0 mg/cm^2 at the nominal operating temperature (16 K) and pressure (0.8 atm).

3.4. Heat radiation shield

The heat radiation shield (Fig. 6) served to protect the target cell and the adjacent materials inside from thermal radiation of the vacuum chamber. It was a tube of the A6061 aluminum alloy with a diameter of 90 mm and with a thickness of 3 mm. The upstream side of the shield had an opening of 26 mm in diameter. The size of this opening was chosen to balance the transmission of beam particles toward the target and the efficiency of radiation shielding. The larger size of 26 mm than the target aperture (20 mm in diameter) was adopted since it is difficult to align the target and the heat radiation with precision. When the target system is cooled down, the parts connected to the first cooling stage (target) and to the second cooling stage (heat radiation shield) shrink by different lengths, which depend on the temperatures and materials. We thus adopted a conservative margin of 6 mm in diameter to ensure the transmission. The downstream side had a rectangular opening with cross sectional area of 80×100 mm^2 to let particles scattered at large angles escape. To limit thermal radiation through these openings, they were covered by 2-μm-thick aluminized Mylar foils. These foils were attached to the radiation shield by the APIEZON N cryogenic high vacuum grease. We also tested a 7-μm-thick aluminum foil. The liquefaction was successful in both cases. Therefore we adopted 2-μm-thick aluminized Mylar foils for smaller energy losses of the incoming beam particles and outgoing scattered particles.

4. Experiments

4.1. Liquefaction test

We performed a test of the new target cell to confirm the liquefaction. The test was carried out at RIBF using

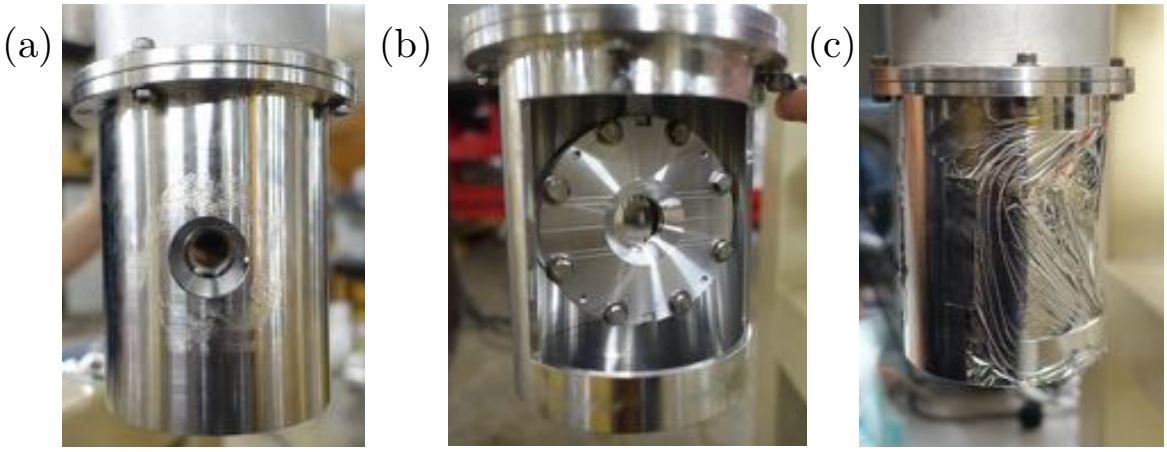

Figure 6: Photographs of the heat radiation shield taken from (a) the upstream side and (b) the downstream side. Photograph (c) was also taken from the downstream side, but the rectangular cut to the radiation shield is covered by an aluminized Mylar foil.

the test bench for cryogenic targets. The target system was installed in the same vacuum chamber used for the measurement of the uniformity of the window foils described in the previous section. The vacuum was kept at 2.0×10^{-7} mbar by using a turbo molecular pump. One of the window foils was replaced with a transparent 125-μm-thick Kapton foil to visually confirm the liquid level inside the cell. During the liquefaction, the temperatures of the upper part of the target cell (thermometer A) and near the window aperture (thermometer B) were monitored. The pressure of hydrogen gas was also measured. The temperature records of thermometer A and B are shown in Fig. 7 together with the pressure record. Before $t = 0$ min, the heater was regulated to keep the temperature A at 15.5 K to avoid solidification of hydrogen below the melting point (R_1). We started introducing hydrogen gas at $t = 0$ min. When hydrogen gas was introduced by gradually opening the valve on the gas handling panel, the temperature of the target rapidly increased to 21 K (R_2). This is because the cooling power of the cryogenic system was not sufficient to remove the heat of condensation released by hydrogen gas undergoing rapid cooling. At the end of R_2, the valve was fully opened and both temperatures A and B stopped increasing. The temperatures as well as the hydrogen gas pressure were decreasing over next 10 minutes. During this period, liquid hydrogen started filling the volume inside the window aperture. The liquid surface emerged from the bottom of the cell. The liquid level gradually grew upwards, but stopped at one point in the middle of the cell as shown in top left of Fig. 7 and the complete filling never happened during R_3. After filling of the opening area stalled, the gas pressure continued to decrease. This indicates that liquefaction slowly but continuously proceeded albeit the liquid level was unchanged. Liquefied hydrogen was most likely remained in the buffer volume unseen from the outside. The temperatures then suddenly started to drop (R_4). This indicates that the liquefaction in the buffer volume came to an end and stopped releasing heat of condensation. The rate of temperature decrease got slower over the time and the temperature curve B followed a gentle slope toward around 16 K. We observed a sudden rise and fall in the temperature A as indicated by the red arrow in Fig. 7 (a) at $t = 9.2$ min. At the same moment, from the glass view port, it was visually observed that the liquid surface level, of which the growth was once stalled in R_3, suddenly raised to the upper end of the aperture volume of the target cell as shown in top and right of Fig. 7. The reason why the aperture volume was suddenly filled out in R_4 and did not undergo gradual and continuous filling together with the buffer volume in R_3 is that the window foils were not cold enough in R_3. The foils underwent cooling in R_4 and the temperature finally decreased below the boiling temperature, which triggered the complete filling in a short period of time. Thermometer A at the upper part of the target cell picked up a signal from the filling likely because the same amount of hydrogen gas was liquefied to compensate liquid hydrogen leaking into the aperture volume. To establish stable operating condition, the temperature was kept above the boiling point of hydrogen by using the heater after R_4.
From the test with the Kapton foil, the observation of the spike signal in thermometer A after filling of the buffer volume confirms the filling of the aperture volume even if it is impossible to visually confirm the liquid level in-

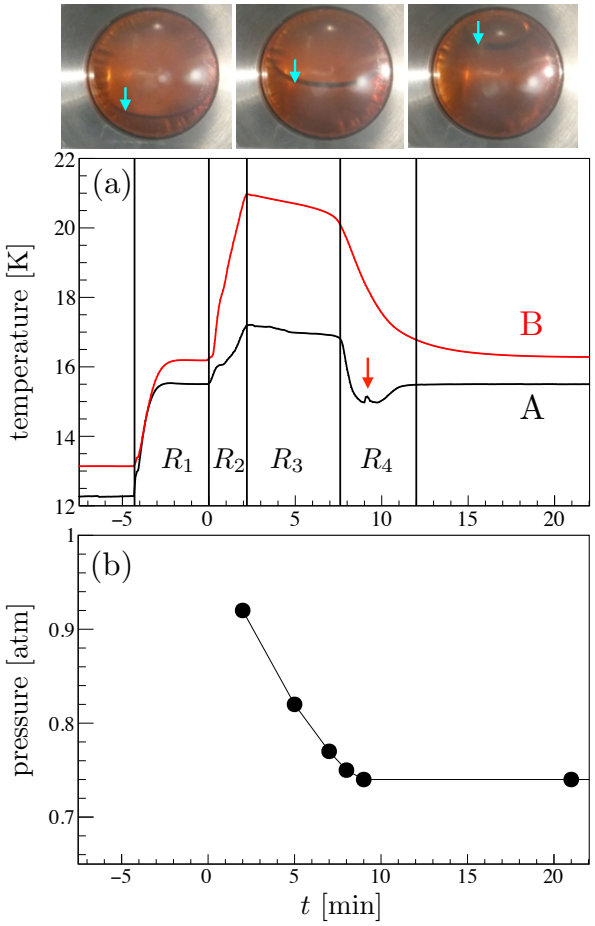

Figure 7: Record of (a) temperatures and (b) pressure during the liquefaction operation in the test chamber. The temperatures measured by thermometer A and B are plotted in black and red, respectively. A sudden rise and fall in temperature observed by thermometer A is indicated by the red arrow. One of the window foils was replaced with a transparent 125-μm-thick Kapton foil. The inside of the cell was photographed through this Kapton foil. From left to right, the photographs taken at t = 5.0, 9.2, and 9.5 min, respectively, are shown. The surface level of liquid hydrogen is indicated by the light blue arrows.

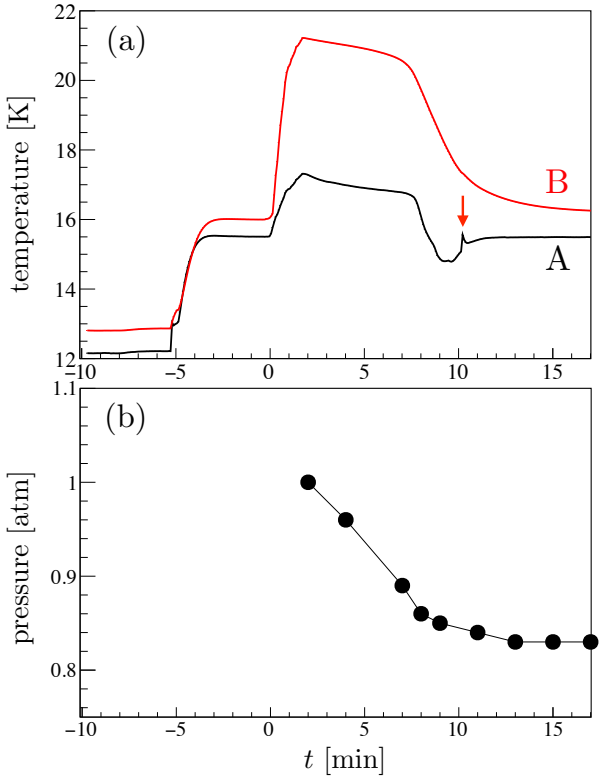

Figure 8: Record of (a) temperatures and (b) pressure during the liquefaction operation in the test chamber. Both window foils were made of HAVAR.

side the cell.

The same test was performed with HAVAR foils on both sides of the target cell. The temperature records of thermometer A and B are shown in Fig. 8 together with the pressure record. The monitored temperatures of both thermometers show the same trend as observed in the previous test with the Kapton foil. The spike signal is clearly visible at t =10.5 min with thermometer A, which is close to the time of the complete filling observed in the previous test. This confirms that the target cell, both the buffer volume and the narrow aperture volume, was fully filled with liquid hydrogen.

4.2. *In-beam test with a ^{12}C beam*

We performed a test with a beam to confirm the liquefaction under experimental conditions and also to evaluate the performance of missing mass spectroscopy using the present target. The in-beam test was carried out at the LISE beam line of GANIL [42]. The setup of the experiment was almost the same as the experiment reported in Ref. [22]. The liquid hydrogen target was installed in a vacuum chamber with 1.2 m in diameter and 1 m in height, called M2C chamber, placed at the D6 experimental station of LISE. The temperature record in the M2C chamber is compared to that of the test chamber in Fig. 9. The cooling started at t = 0. In the test chamber, the temperatures leveled off after 12 hours of cooling. The M2C chamber follows the same decreasing trend as the test chamber, but it turned to an increasing trend at t = 8 h and leveled off at a much higher temperature at t = 16 h. This is attributed to the fact that the M2C chamber has a much larger volume (1,130 L) than the test chamber (18 L) and a worse

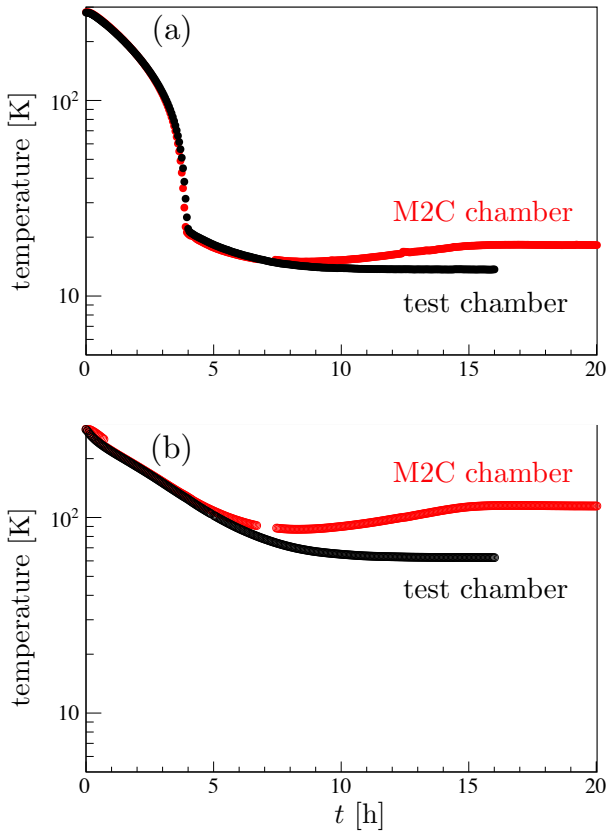

Figure 9: Temperatures of (a) thermometer A and (b) thermometer C during the liquefaction operation in the M2C chamber (red). For comparison, the same data of the test chamber (black) is added.

vacuum level. The vacuum pressure of the M2C chamber equipped with three turbo molecular pumps and a cryogenic pump was 2.0×10^{-6} mbar. This is about one order of magnitude worse than the vacuum level in the test chamber. Residual gas molecules are accumulated on to the body frame and to the windows of the target as the cooling continues. This results in an increasingly lower reflection coefficient of these materials. As the reflection coefficient decreases, the materials absorb more radiant heat, thus increasing the temperature. During the beam time, we sometimes warmed up the target to force the material surfaces outgassing.

The ^{12}C beam was accelerated by a pair of cyclotrons. The energy of 75 MeV/u at the exit of the second cyclotron was degraded to 54.4 MeV/u by using the 2,156-μm-thick Be primary target and the 2,180-μm-thick Be degrader of the LISE spectrometer. The intensity of the ^{12}C beam was limited to 100 kpps to avoid damage to the tracking detectors. Two multiwire proportional chambers CATSs [43] with 0.5 mm position resolution were placed 118.70 cm and 67.85 cm, respectively, upstream of the liquid hydrogen target to measure the position of beam particles. The incident position and angle on the liquid hydrogen target was deduced by extrapolating the positions measured by the CATS detectors. The charged particle telescope MUST2 [27] was used to detect recoiling deuterons. An array of six telescopes was placed downstream of the liquid hydrogen target. The distance between the target and the front surface of MUST2 was set to 30 cm to detect scattered particles from 2° up to 35° with respect to the beam axis. The MUST2 telescopes consist of a DSSD followed by CsI(Tl) detectors. The DSSD has an active area of 98×98 mm^2 with a thickness of 300 μm. Each side of the detector is segmented into 128 strips with a 0.76 mm pitch. The energy resolution is about 40 keV FWHM for 5.5-MeV α particles of an ^{241}Am standard source. Behind the DSSD, 16 CsI(Tl) crystals in a 4×4 matrix cover an area of 122×122 mm^2. The DSSD provides the energy loss and detection position of hit particles, while the CsI(Tl) detectors with a thickness of 40 mm measure the residual energy. The total kinetic energy is deduced from the sum of the energies measured by the DSSD and the CsI(Tl) detectors. The particle identification was performed by the $E-\Delta E$ method. The scattering angle of a recoiling particle was obtained from the hit position measured by the MUST2 telescopes and the incident position and angle of the beam by CATS.

In the setup of the M2C chamber, the inside of the target cell is invisible from outside due to the use of non-transparent HAVAR foils. While the thermometers signal when the aperture volume is filled during the liquefaction of hydrogen gas as described in the previous section, it does not help continuously monitor the status of liquid hydrogen inside the cell as to whether liquid always fills the volume or starts to evaporate at a certain point. It is therefore more reliable and secure if one can visually confirm the liquid level throughout operation. During the test, we noticed that the beam profile image at the target cell position, deduced from the trajectory data of CATS, can be used for this purpose. Examples of beam profile images are shown in Fig. 10. The data are selected for the events with at least one hit in any MUST2 telescopes. This condition helps select scattering events off proton targets, thus increasing the sensitivity to hydrogen atoms in the cell. The liquid level inside the circular aperture is visible in these images taken when the volume is (a) fully filled, (b) partially filled and (c) empty. Note that loci are seen at the periphery of the circular aperture in these images. These were made by beam particles scattered off the edge of the window frame. Throughout the experiment, we used

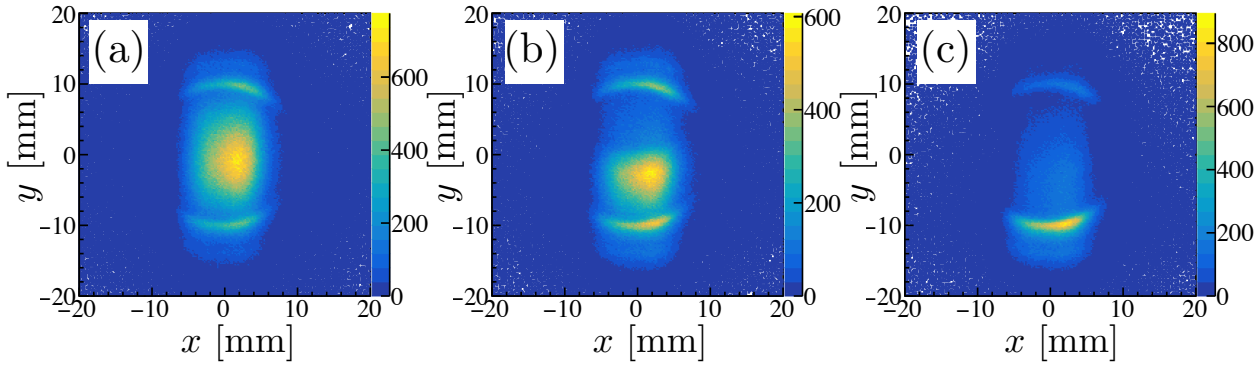

Figure 10: Beam profile at the target cell position obtained from the CATS detectors. The events with a scattered particle hitting one of the MUST2 telescopes were selected to increase the sensitivity to protons inside the cell. More particles are scattered by the edge of the alminium window, thus two rings are seen at 10 mm from the center of the target. The target cell is (a) fully filled, (b) partially filled, and (c) empty.

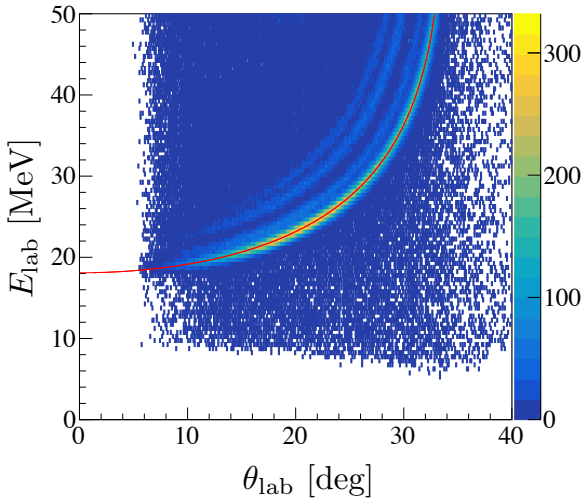

Figure 11: Scatter plot of total kinetic energies against emission angles of deuteron particles from the ^{12}C$(p,d)^{11}$C reaction at 54.4 MeV/u. The kinematics curve for the ground state of ^{11}C is shown by the red curve.

this method to monitor the liquid level inside the target cell.

The excitation energy spectrum was obtained from the kinetic energies and the scattering angles of the deutrons as shown in Fig. 11 by the missing mass method in the same way as Ref. [22]. The obtained spectrum of the ^{12}C$(p,d)^{11}$C reaction is shown in Fig. 12. Four peaks are seen at around 0, 2.0, 4.5 and 6.5 MeV, respectively. The peaks at 0 MeV and 2.0 MeV correspond to the ground state and the $1/2^-$ excited state at 2.00 MeV, respectively. The peaks at 4.5 and 6.5 MeV are both composite of a few states, the $5/2^-$ (4.32 MeV) and $3/2^-$ (4.80 MeV) for the former and the $1/2^+$ (6.34 MeV), $7/2^-$ (6.48 MeV) and $5/2^+$ (6.90 MeV) states for the latter.

The resolution of excitation energies was evaluated by fitting the spectrum with four Gaussian functions and a linear function for the background. The obtained resolution of 500 keV r.m.s. for the ground state of ^{11}C agrees with the resolution estimated by Monte Carlo simulations, which took into account all materials around the target as well as the experimental parameters such as the spatial and angular spreads of the beam or the energy and position resolutions of the detectors.

The differential cross sections of the ground state and the first excited state of ^{11}C were deduced and are plotted in Fig. 13. The thickness of 1.21(13) mm, or 8.47(91) mg/cm^2, was adopted to calculate the differential cross sections. Note that the adopted thickness was averaged over the area of the actual beam spot, and not over the entire area of the opening. The uncertainty of the thickness is deduced from the root mean square value of two contributions. One is the spatial resolution of the laser measurement (±0.1 mm). The other arises from the uncertainty of the measured beam profile on the target (±0.08 mm). The absolute cross sections are compared to the previous results obtained with a proton beam at 57 [40] and 61 MeV [41], respectively. The corresponding center-of-mass energies of 52.5 and 56.1 MeV, respectively, are close to that of the present reaction energy (50.4 MeV) using the ^{12}C beam at 54.4 MeV/u. The angular distributions of both ground and excited states are comparable to the earlier results. The agreement confirms the assumed thickness of 1.21 mm.

5. Conclusion

We developed a new liquid hydrogen target with a thin thickness (1.5 mm at the center) and a wide opening (20 mm in diameter) to perform missing mass experiments with RI beams. A target cell and a heat shield

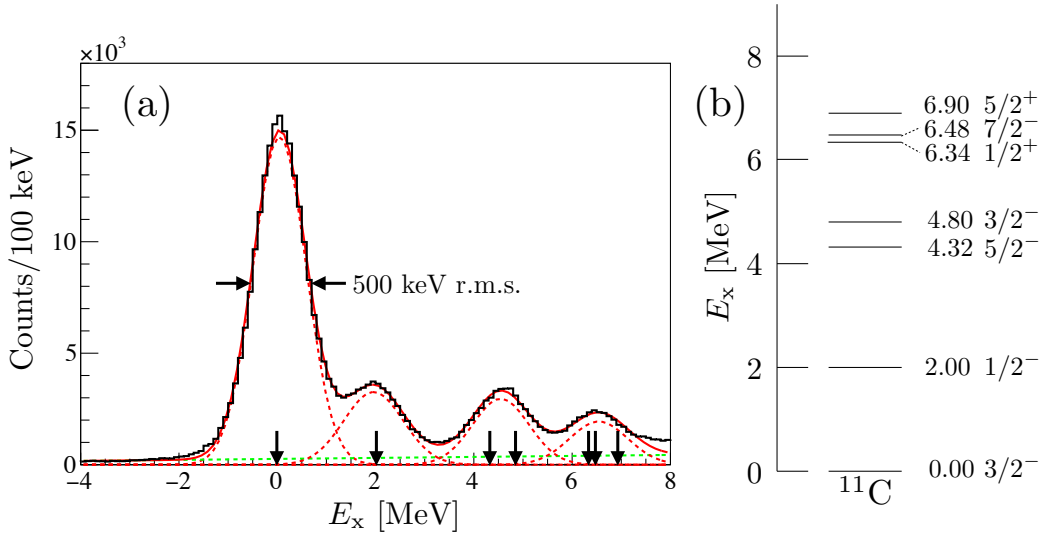

Figure 12: Excitation energy spectrum of ^{11}C from the ^{12}C$(p,d)^{11}$C reaction with a 54.4 MeV/u ^{12}C beam. The known ground and excited states of ^{11}C are indicated by the arrows. The level scheme of ^{11}C up to 7 MeV [39] is shown in the Fig. (b).

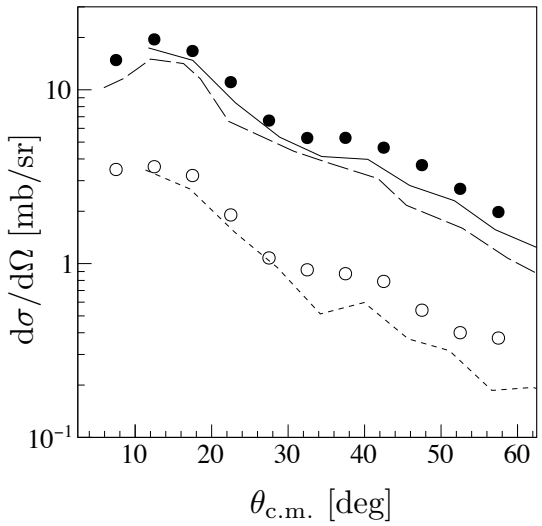

Figure 13: Differential cross sections leading to the ground $3/2^-$ state (full circles) and $1/2^-$ state at 2.0 MeV (open circles) from the ^{12}C$(p,d)^{11}$C reaction with a 54.4 MeV/u ^{12}C beam. The solid (ground state) and dotted ($1/2^-$ state) lines denote the results measured at an incident energy of 57 MeV [40] while the dashed line (ground state) denotes the the result of 61 MeV [41].

were designed to minimize the cooling loss due to thermal radiation from the vacuum chamber. The cooling test at the test bench of RIBF showed that the liquefaction went well and liquefied hydrogen filled the entire volume of the target cell including the narrow volume in the opening. We also established two methods to monitor the status of the filling inside the target cell without visually inspecting from the outside, one relying on the temperature monitor and the other on the reaction rate of beam particles. The liquid hydrogen target was tested with a ^{12}C beam at GANIL. Missing mass spectroscopy was carried out by using the charged particle telescopes MUST2. The excitation energy and the cross sections were obtained from the measurement of recoiling particles. The excitation energy resolution for the ground state of ^{11}C populated by the ^{12}C$(p,d)^{11}$C reaction was obtained to be 500 keV r.m.s., which was confirmed to be in line with the simulation that we carried out. The thickness of 1.21(13) mm (8.47(91) mg/cm^2) was adopted by taking the beam profile into consideration. The differential cross sections reproduced the absolute values of the previous results at almost the same incident energies.

Acknowledgements

The authors thank the technical staff members of GANIL, V. Morel, S. Le Moal and F. Pillon, for their assistance for the installation, preparation and operation of the target at GANIL. They thank the collaborators of the E738 experiment for the collection of the data. S. K. was supported by the JSPS Grant-in-Aid for JSPS Research Fellows JP16J04726.

References

[1] I. Tanihata, H. Hamagaki, O. Hashimoto, Y. Shida, N. Yoshikawa, K. Sugimoto, O. Yamakawa, T. Kobayashi, N. Takahashi, Measurements of interaction cross sections and nuclear radii in the light p-shell region, Phys. Rev. Lett. 55 (1985) 2676–2679. doi:10.1103/PhysRevLett.55.2676.

URL https://link.aps.org/doi/10.1103/PhysRevLett.55.2676

[2] O. Sorlin, M.-G. Porquet, Nuclear magic numbers: New features far from stability, Prog. Part. Nucl. Phys. 61 (2) (2008) 602 – 673. doi:https://doi.org/10.1016/j.ppnp.2008.05.001.
URL http://www.sciencedirect.com/science/article/pii/S0146641008000380

[3] S. Gales, GANIL-SPIRAL2: a new era, J. of Phys.: Conference Series 267 (2011) 012009. doi:10.1088/1742-6596/267/1/012009.
URL https://doi.org/10.1088%2F1742-6596%2F267%2F1%2F012009

[4] M. Durante, P. Indelicato, B. Jonson, V. Koch, K. Langanke, U.-G. Meißner, E. Nappi, T. Nilsson, T. Stöhlker, E. Widmann, M. Wiescher, All the fun of the FAIR: fundamental physics at the facility for antiproton and ion research, Phys. Script. 94 (3) (2019) 033001. doi:10.1088/1402-4896/aaf93f.
URL https://doi.org/10.1088%2F1402-4896%2Faaf93f

[5] A. B. Balantekin, J. Carlson, D. J. Dean, G. M. Fuller, R. J. Furnstahl, M. Hjorth-Jensen, R. V. F. Janssens, B.-A. Li, W. Nazarewicz, F. M. Nunes, W. E. Ormand, S. Reddy, B. M. Sherrill, Nuclear theory and science of the facility for rare isotope beams, Mod. Phys. Lett. A 29 (11) (2014) 1430010. doi:10.1142/S0217732314300109.
URL https://doi.org/10.1142/S0217732314300109

[6] J. Yang, J. Xia, G. Xiao, H. Xu, H. Zhao, X. Zhou, X. Ma, Y. He, L. Ma, D. Gao, J. Meng, Z. Xu, R. Mao, W. Zhang, Y. Wang, L. Sun, Y. Yuan, P. Yuan, W. Zhan, J. Shi, W. Chai, D. Yin, P. Li, J. Li, L. Mao, J. Zhang, L. Sheng, High intensity heavy ion accelerator facility (hiaf) in china, Nucl. Instrum. and Meth. B 317 (2013) 263 – 265. doi:https://doi.org/10.1016/j.nimb.2013.08.046.
URL http://www.sciencedirect.com/science/article/pii/S0168583X13009877

[7] P. Reiter, N. Warr, Nuclear structure studies with re-accelerated beams at rex-and hie-isolde, Prog. Part. Nucl. Phys. 113 (2020) 103767. doi:https://doi.org/10.1016/j.ppnp.2020.103767.
URL http://www.sciencedirect.com/science/article/pii/S0146641020300144

[8] H. Sakurai, Ri beam factory project at riken, Nucl. Phys. A 805 (1) (2008) 526c – 532c, iNPC 2007. doi:https://doi.org/10.1016/j.nuclphysa.2008.02.291.
URL http://www.sciencedirect.com/science/article/pii/S0375947408003862

[9] DWUCK4 and DWUCK5 codes.
URL https://people.nscl.msu.edu/brown/reaction-codes/.

[10] University of Surrey version of the code TWOFNR.
URL http://nuclear theory.eps.surrey.ac.uk/NPG/code.htm

[11] I. J. Thompson, Coupled reaction channels calculations in nuclear physics, Comp. Phys. Rep. 7 (4) (1988) 167 – 212. doi:https://doi.org/10.1016/0167-7977(88)90005-6.
URL http://www.sciencedirect.com/science/article/pii/0167797788900056

[12] A. de Vismes, P. Roussel-Chomaz, W. Mittig, A. Pakou, N. Alamanos, J.-C. Angélique, F. Auger, J. Barrette, E. Bauge, A. Belozyorov, C. Borcea, F. Carstoiu, W. Catford, M.-D. Cortina-Gil, J.-P. Delaroche, Z. Dlouhy, A. Gillibert, M. Girod, D. Hirata, V. Lapoux, A. Lepine-Szily, S. Lukyanov, F. Marie, A. Musumarra, F. de Oliveira, N. Orr, S. Ottini-Hustache, Y. Penionzhkevich, F. Sarazin, H. Savajols, N. Skobelev, Proton reaction cross-section measurements on stable and neutron-rich nuclei as a probe of the nucleon–nucleus interaction, Nucl. Phys. A 706 (3) (2002) 295 – 312. doi:https://doi.org/10.1016/S0375-9474(02)00753-4.
URL http://www.sciencedirect.com/science/article/pii/S0375947402007534

[13] S. Ishimoto, T. Kobayashi, K. Morimoto, I. Nomura, A. Ozawa, S. Suzuki, Y. Takahashi, I. Tanihata, T. Tsuru, Windowless solid hydrogen target, Nucl. Instrum. and Meth. A 480 (2) (2002) 304 – 314. doi:https://doi.org/10.1016/S0168-9002(01)00951-2.
URL http://www.sciencedirect.com/science/article/pii/S0168900201009512

[14] H. Ryuto, M. Kunibu, T. Minemura, T. Motobayashi, K. Sagara, S. Shimoura, M. Tamaki, Y. Yanagisawa, Y. Yano, Liquid hydrogen and helium targets for radioisotope beams at riken, Nucl. Instrum. and Meth. A 555 (1) (2005) 1 – 5. doi:https://doi.org/10.1016/j.nima.2005.08.102.
URL http://www.sciencedirect.com/science/article/pii/S016890020501778X

[15] P. Dolégiéviez, A. Gillibert, W. Mittig, X. Mougeot, A. Obertelli, F. de Oliveira, M. Ozille, P. Robillard, P. Roussel-Chomaz, H. Savajols, A cryogenic target for direct reaction studies with exotic beams, Nuclear Instruments and Methods in Physics Research Section A: Accelerators, Spectrometers, Detectors and Associated Equipment 564 (1) (2006) 32 – 37. doi:https://doi.org/10.1016/j.nima.2006.03.027.
URL http://www.sciencedirect.com/science/article/pii/S0168900206005481

[16] Y. Matsuda, H. Sakaguchi, J. Zenihiro, S. Ishimoto, S. Suzuki, H. Otsu, T. Ohnishi, H. Takeda, K. Ozeki, K. Tanaka, S. Terashima, Y. Maeda, T. Kobayashi, A. Koreeda, K. Kamei, Large, thin solid hydrogen target using para-h2, Nucl. Instrum. and Meth. A 643 (1) (2011) 6 – 10. doi:https://doi.org/10.1016/j.nima.2011.04.017.
URL http://www.sciencedirect.com/science/article/pii/S0168900211007558

[17] A. Gillibert, A. Corsi, F. Flavigny, C. Louchart, L. Nalpas, A. Obertelli, E. C. Pollacco, G. Authelet, J. M. Gheller, D. Guillaume, V. Méot, O. Roig, I. Vinyar, A. Lukin, Windowless thin solid-hydrogen target: Chymene, Eur. Phys. J. A 49 (155) (2013) 12.
URL https://doi.org/10.1140/epja/i2013-13155-y

[18] A. Obertelli, A. Delbart, S. Anvar, L. Audirac, G. Authelet, H. Baba, B. Bruyneel, D. Calvet, F. Château, A. Corsi, P. Doornenbal, J. M. Gheller, A. Giganon, C. Lahonde-Hamdoun, D. Leboeuf, D. Loiseau, A. Mohamed, J. P. Mols, H. Otsu, C. Péron, A. Peyaud, E. C. Pollacco, G. Prono, J. Y. Rousse, C. Santamaria, T. Uesaka, Minos: A vertex tracker coupled to a thick liquid-hydrogen target for in-beam spectroscopy of exotic nuclei, Eur. Phys. J. A 50 (1) (2014) 45.
URL https://doi.org/10.1140/epja/i2014-14008-y

[19] C. Louchart, J. Gheller, P. Chesny, G. Authelet, J. Rousse, A. Obertelli, P. Boutachkov, S. Pietri, F. Ameil, L. Audirac, A. Corsi, Z. Dombradi, J. Gerl, A. Gillibert, W. Korten, C. Mailleret, E. Merchan, C. Nociforo, N. Pietralla, D. Ralet, M. Reese, V. Stepanov, The prespec liquid-hydrogen target for in-beam gamma spectroscopy of exotic nuclei at gsi, Nucl. Instrum. and Meth. A 736 (2014) 81 – 87. doi:https://doi.org/10.1016/j.nima.2013.10.035.
URL http://www.sciencedirect.com/science/article/pii/S0168900213014150

[20] R. Kanungo, Iris: The isac charged particle reaction spectroscopy facility for reaccelerated high-energy isol beams, Hyperfine Interactions 225 (2014) 235. doi:10.1007/s10751-013-0904-8.

URL https://doi.org/10.1007/s10751-013-0904-8

[21] L. Gaudefroy, O. Sorlin, D. Beaumel, Y. Blumenfeld, Z. Dombrádi, S. Fortier, S. Franchoo, M. Gélin, J. Gibelin, S. Grévy, F. Hammache, F. Ibrahim, K. W. Kemper, K.-L. Kratz, S. M. Lukyanov, C. Monrozeau, L. Nalpas, F. Nowacki, A. N. Ostrowski, T. Otsuka, Y.-E. Penionzhkevich, J. Piekarewicz, E. C. Pollacco, P. Roussel-Chomaz, E. Rich, J. A. Scarpaci, M. G. St. Laurent, D. Sohler, M. Stanoiu, T. Suzuki, E. Tryggestad, D. Verney, Reduction of the spin-orbit splittings at the $n = 28$ shell closure, Phys. Rev. Lett. 97 (2006) 092501. doi:10.1103/PhysRevLett.97.092501.
URL https://link.aps.org/doi/10.1103/PhysRevLett.97.092501

[22] D. Suzuki, H. Iwasaki, D. Beaumel, M. Assié, H. Baba, Y. Blumenfeld, F. de Oliveira Santos, N. de Séréville, A. Drouart, S. Franchoo, J. Gibelin, A. Gillibert, S. Giron, S. Grévy, J. Guillot, M. Hackstein, F. Hammache, N. Keeley, V. Lapoux, F. Maréchal, A. Matta, S. Michimasa, L. Nalpas, F. Naqvi, H. Okamura, H. Otsu, J. Pancin, D. Y. Pang, L. Perrot, C. M. Petrache, E. Pollacco, A. Ramus, W. Rother, P. Roussel-Chomaz, H. Sakurai, J.-A. Scarpaci, O. Sorlin, P. C. Srivastava, I. Stefan, C. Stodel, Y. Tanimura, S. Terashima, Second 0^+ state of unbound ^{12}O: Scaling of mirror asymmetry, Phys. Rev. C 93 (2016) 024316. doi:10.1103/PhysRevC.93.024316.
URL https://link.aps.org/doi/10.1103/PhysRevC.93.024316

[23] J. Lee, M. Tsang, D. Bazin, D. Coupland, V. Henzl, D. Henzlova, M. Kilburn, W. G. Lynch, A. M. Rogers, A. Sanetullaev, Z. Y. Sun, M. Youngs, R. J. Charity, L. G. Sobotka, M. Famiano, S. Hudan, D. Shapira, P. O'Malley, W. A. Peters, K. Y. Chae, K. Schmitt, Neutron spectroscopic factors of ^{34}Ar and ^{46}Ar from (p, d) transfer reactions, Phys. Rev. C 83 (2011) 014606. doi:10.1103/PhysRevC.83.014606.
URL https://link.aps.org/doi/10.1103/PhysRevC.83.014606

[24] B. B. Back, S. I. Baker, B. A. Brown, C. M. Deibel, S. J. Freeman, B. J. DiGiovine, C. R. Hoffman, B. P. Kay, H. Y. Lee, J. C. Lighthall, S. T. Marley, R. C. Pardo, K. E. Rehm, J. P. Schiffer, D. V. Shetty, A. W. Vann, J. Winkelbauer, A. H. Wuosmaa, First experiment with helios: The structure of ^{13}**B**, Phys. Rev. Lett. 104 (2010) 132501. doi:10.1103/PhysRevLett.104.132501.
URL https://link.aps.org/doi/10.1103/PhysRevLett.104.132501

[25] W. N. Catford, C. N. Timis, R. C. Lemmon, M. Labiche, N. A. Orr, B. Fernández-Domínguez, R. Chapman, M. Freer, M. Chartier, H. Savajols, M. Rejmund, N. L. Achouri, N. Amzal, N. I. Ashwood, T. D. Baldwin, M. Burns, L. Caballero, J. M. Casadjian, N. Curtis, G. de France, W. Gelletly, X. Liang, S. D. Pain, V. P. E. Pucknell, B. Rubio, O. Sorlin, K. Spohr, C. Theisen, D. D. Warner, Migration of nuclear shell gaps studied in the $d(^{24}\mathrm{Ne}, p\gamma)^{25}$Ne reaction, Phys. Rev. Lett. 104 (2010) 192501. doi:10.1103/PhysRevLett.104.192501.
URL https://link.aps.org/doi/10.1103/PhysRevLett.104.192501

[26] Y. Blumenfeld, F. Auger, J. Sauvestre, F. Maréchal, S. Ottini, N. Alamanos, A. Barbier, D. Beaumel, B. Bonnereau, D. Charlet, J. Clavelin, P. Courtat, P. Delbourgo-Salvador, R. Douet, M. Engrand, T. Ethvignot, A. Gillibert, E. Khan, V. Lapoux, A. Lagoyannis, L. Lavergne, S. Lebon, P. Lelong, A. Lesage, V. Ven, I. Lhenry, J. Martin, A. Musumarra, S. Pita, L. Petizon, E. Pollacco, J. Pouthas, A. Richard, D. Rougier, D. Santonocito, J. Scarpaci, J. Sida, C. Soulet, J. Stutzmann, T. Suomijärvi, M. Szmigiel, P. Volkov, G. Voltolini, Must: A silicon strip detector array for radioactive beam experiments, Nucl. Instrum. and Meth. A 421 (3) (1999) 471 – 491. doi:https://doi.org/10.1016/S0168-9002(98)01178-4.
URL http://www.sciencedirect.com/science/article/pii/S0168900298011784

[27] E. Pollacco, D. Beaumel, P. Roussel-Chomaz, E. Atkin, P. Baron, J. Baronick, E. P. Becheva, Y. Blumenfeld, A. Boujrad, A. Drouart, F. Druillole, P. Edelbruck, M. Gelin, A. Gillibert, C. Houarner, V. Lapoux, L. Lavergne, L. Leberthe, G.and Leterrier, V. Le Ven, F. Lugiez, L. Nalpas, L. Olivier, B. Paul, B. Raine, A. Richard, M. Rouger, F. Saillant, F. Skaza, M. Tripon, M. Vilmay, E. Wanlin, M. Wittwer, Must2: A new generation array for direct reaction studies, Eur. Phys. J. A Supplement 1 (287) (2005) 287. doi:10.1140/epjad/i2005-06-162-5.
URL https://doi.org/10.1140/epjad/i2005-06-162-5

[28] M. Wallace, M. Famiano, M.-J. van Goethem, A. Rogers, W. Lynch, J. Clifford, F. Delaunay, J. Lee, S. Labostov, M. Mocko, L. Morris, A. Moroni, B. Nett, D. Oostdyk, R. Krishnasamy, M. Tsang, R. de Souza, S. Hudan, L. Sobotka, R. Charity, J. Elson, G. Engel, The high resolution array (hira) for rare isotope beam experiments, Nucl. Instrum. and Meth. A 583 (2) (2007) 302 – 312. doi:https://doi.org/10.1016/j.nima.2007.08.248.
URL http://www.sciencedirect.com/science/article/pii/S016890020701947X

[29] J. Lighthall, B. Back, S. Baker, S. Freeman, H. Lee, B. Kay, S. Marley, K. Rehm, J. Rohrer, J. Schiffer, D. Shetty, A. Vann, J. Winkelbauer, A. Wuosmaa, Commissioning of the helios spectrometer, Nucl. Instrum. and Meth. A 622 (1) (2010) 97 – 106. doi:https://doi.org/10.1016/j.nima.2010.06.220.
URL http://www.sciencedirect.com/science/article/pii/S0168900210014105

[30] M. Labiche, W. Catford, R. Lemmon, C. Timis, R. Chapman, N. Orr, B. Fernández-Domínguez, G. Moores, N. Achouri, N. Amzal, S. Appleton, N. Ashwood, T. Baldwin, M. Burns, L. Caballero, J. Cacitti, J. Casadjian, M. Chartier, N. Curtis, K. Faiz, G. de France, M. Freer, J. Gautier, W. Gelletly, G. Iltis, B. Lecornu, X. Liang, C. Marry, Y. Merrer, L. Olivier, S. Pain, V. Pucknell, B. Raine, M. Rejmund, B. Rubio, F. Saillant, H. Savajols, O. Sorlin, K. Spohr, C. Theisen, G. Voltolini, D. Warner, Tiara: A large solid angle silicon array for direct reaction studies with radioactive beams, Nucl. Instrum. and Meth. A 614 (3) (2010) 439 – 448. doi:https://doi.org/10.1016/j.nima.2010.01.009.
URL http://www.sciencedirect.com/science/article/pii/S0168900210000379

[31] Y. Yanagisawa, M. Notani, H. Sakurai, M. Kunibu, H. Akiyoshi, N. Aoi, H. Baba, K. Demichi, N. Fukuda, H. Hasegawa, Y. Higurashi, M. Ishihara, N. Iwasa, H. Iwasaki, T. Gomi, S. Kanno, M. Kurokawa, Y. Matsuyama, S. Michimasa, T. Minemura, T. Mizoi, T. Nakamura, A. Saito, M. Serata, S. Shimoura, T. Sugimoto, E. Takeshita, S. Takeuchi, K. Ue, K. Yamada, K. Yoneda, T. Motobayashi, The first excited state of ^{30}Ne studied by proton inelastic scattering in reversed kinematics, Phys. Lett. B 566 (1) (2003) 84 – 89. doi:https://doi.org/10.1016/S0370-2693(03)00802-5.
URL http://www.sciencedirect.com/science/article/pii/S0370269303008025

[32] N. Iwasa, T. Motobayashi, H. Sakurai, H. Akiyoshi, Y. Ando, N. Aoi, H. Baba, N. Fukuda, Z. Fülöp, U. Futakami, T. Gomi, Y. Higurashi, K. Ieki, H. Iwasaki, T. Kubo, S. Kubono, H. Kinugawa, H. Kumagai, M. Kunibu, S. Michimasa, T. Minemura, H. Murakami, K. Sagara, A. Saito, S. Shimoura,

S. Takeuchi, Y. Yanagisawa, K. Yoneda, M. Ishihara, In-beam γ spectroscopy of ^{34}Si with deuteron inelastic scattering using reverse kinematics, Phys. Rev. C 67 (2003) 064315. doi:10.1103/PhysRevC.67.064315.
URL https://link.aps.org/doi/10.1103/PhysRevC.67.064315

[33] S. Takeuchi, N. Aoi, T. Motobayashi, S. Ota, E. Takeshita, H. Suzuki, H. Baba, T. Fukui, Y. Hashimoto, K. Ieki, N. Imai, H. Iwasaki, S. Kanno, Y. Kondo, T. Kubo, K. Kurita, T. Minemura, T. Nakabayashi, T. Nakamura, T. Okumura, T. K. Onishi, H. Sakurai, S. Shimoura, R. Sugou, D. Suzuki, M. K. Suzuki, M. Takashina, M. Tamaki, K. Tanaka, Y. Togano, K. Yamada, Low-lying states in ^{32}Mg studied by proton inelastic scattering, Phys. Rev. C 79 (2009) 054319. doi:10.1103/PhysRevC.79.054319.
URL https://link.aps.org/doi/10.1103/PhysRevC.79.054319

[34] Y. Kondo, T. Nakamura, Y. Satou, T. Matsumoto, N. Aoi, N. Endo, N. Fukuda, T. Gomi, Y. Hashimoto, M. Ishihara, S. Kawai, M. Kitayama, T. Kobayashi, Y. Matsuda, N. Matsui, T. Motobayashi, T. Nakabayashi, T. Okumura, H. Ong, T. Onishi, K. Ogata, H. Otsu, H. Sakurai, S. Shimoura, M. Shinohara, T. Sugimoto, S. Takeuchi, M. Tamaki, Y. Togano, Y. Yanagisawa, Low-lying intruder state of the unbound nucleus ^{13}Be, Phys. Lett. B 690 (3) (2010) 245 – 249. doi:https://doi.org/10.1016/j.physletb.2010.05.031.
URL http://www.sciencedirect.com/science/article/pii/S0370269310006234

[35] Y. Satou, T. Nakamura, Y. Kondo, N. Matsui, Y. Hashimoto, T. Nakabayashi, T. Okumura, M. Shinohara, N. Fukuda, T. Sugimoto, H. Otsu, Y. Togano, T. Motobayashi, H. Sakurai, Y. Yanagisawa, N. Aoi, S. Takeuchi, T. Gomi, M. Ishihara, S. Kawai, H. Ong, T. Onishi, S. Shimoura, M. Tamaki, T. Kobayashi, Y. Matsuda, N. Endo, M. Kitayama, ^{14}Be(p,n)^{14}B reaction at 69 MeV in inverse kinematics, Phys. Lett. B 697 (5) (2011) 459 – 462. doi:https://doi.org/10.1016/j.physletb.2011.02.045.
URL http://www.sciencedirect.com/science/article/pii/S0370269311001900

[36] M. M. H. Johnson Michael A, PID Control, New Identification and Design Methods, Springer-Verlag London, 2005.

[37] Data sheet of HAVAR foil.
URL https://shop.nilaco.jp/upload_files/d72lsqbc8f4kgg8kowgw4kk0.pdf

[38] A. Obertelli, T. Uesaka, Hydrogen targets for exotic-nuclei studies developed over the past 10 years, Eur. Phys. J. A 47 (2011) 105. doi:https://doi.org/10.1140/epja/i2011-11105-5.
URL 10.1140/epja/i2011-11105-5

[39] National nuclear data center, https://www.nndc.bnl.gov/.

[40] Y. Ishizaki, K. Kikuchi, K. Matsuda, T. Mikumo, Y. Nakajima, I. Nonaka, Y. Saji, A. Suzuki, H. Yamaguchi, R. Eisberg, An experimental survey of nuclear reactions induced by 57 mev protons part ii (p, d) reactions, J. Phys. Soc. of Japan 20 (12) (1965) 2118–2128. doi:10.1143/JPSJ.20.2118.
URL https://doi.org/10.1143/JPSJ.20.2118

[41] J. R. Comfort, B. C. Karp, Scattering and reaction dynamics for the ^{12}C+p system, Phys. Rev. C 21 (1980) 2162–2176. doi:10.1103/PhysRevC.21.2162.
URL https://link.aps.org/doi/10.1103/PhysRevC.21.2162

[42] R. Anne, A. C. Mueller, Lise 3: a magnetic spectrometer—wien filter combination for secondary radioactive beam production, Nucl. Instrum. and Meth. B 70 (1) (1992) 276 – 285. doi:https://doi.org/10.1016/0168-583X(92)95943-L.
URL http://www.sciencedirect.com/science/article/pii/0168583X9295943L

[43] S. Ottini-Hustache, C. Mazur, F. Auger, A. Musumarra, N. Alamanos, B. C. n, A. Gillibert, A. Lagoyannis, O. Maillard, E. Pollacco, J. Sida, M. Riallot, Cats, a low pressure multiwire proportionnal chamber for secondary beam tracking at ganil, Nucl. Instrum. and Meth. A 431 (3) (1999) 476 – 484. doi:https://doi.org/10.1016/S0168-9002(99)00380-0.
URL http://www.sciencedirect.com/science/article/pii/S0168900299003800